Check for updates

Angewandte Chemie International Edition

Angewandte International Edition Chemie

How to cite: *Angew. Chem. Int. Ed.* **2026**, 65, e9709775
doi.org/10.1002/anie.9709775

RESEARCH ARTICLE OPEN ACCESS

Chlorination-Driven BODIPY Fluorescent Probes for the Selective Monitoring of Myeloperoxidase Activity in Cells and Inflamed Mouse Models

Siyoung Cho[1] | Yongyang Luo[2] | Jeehyeon Bae[3] | Youngmi Kim[1]

[1]Department of Chemistry and Research Institute of Basic Sciences, Kyung Hee University, Seoul, South Korea | [2]Department of Life Science, Chung-Ang University, Seoul, South Korea | [3]School of Pharmacy, Chung-Ang University, Seoul, South Korea

Correspondence: Jeehyeon Bae (jeehyeon@cau.ac.kr) | Youngmi Kim (youngmi.kim@khu.ac.kr)

Received: 6 May 2026 | **Revised:** 20 August 2026 | **Accepted:** 7 September 2026

Keywords: bioimaging | chlorination | fluorescent probes | hypochlorous acid | myeloperoxidase

ABSTRACT

Myeloperoxidase (MPO) generates hypochlorous acid (HOCl), a major oxidant in inflammatory biology and an increasingly recognized pathogenic mediator and therapeutic target in oxidative and inflammatory diseases. However, selective detection of MPO activity remains challenging because most HOCl-responsive fluorescent probes operate through nonspecific oxidative mechanisms, rendering them vulnerable to interference from competing reactive oxygen and nitrogen species. Here, we present an MPO-reporting fluorescent platform based on a *meso*-carboxamide-substituted 3,5-dimethyl BODIPY scaffold that exploits the electrophilic chlorinating reactivity of MPO-derived HOCl. The lead probe undergoes rapid chlorination at the 2,6-positions, generating highly emissive products with ca. 40 nm bathochromic shifts and overcoming the minimal spectral responses and fluorescence quenching that have limited earlier chlorination-based designs. The modular *meso*-carboxamide architecture further allows facile incorporation of targeting motifs without compromising probe performance. This platform enables quantitative MPO assays, cellular imaging of exogenous and endogenous MPO-derived HOCl, discrimination between cancer and normal cells based on redox differences, and noninvasive visualization of MPO-driven inflammation in a mouse model of atopic dermatitis. These results establish electrophilic chlorination as a viable design strategy for selective MPO-responsive fluorescent probes and provide a versatile tool for investigating MPO-associated inflammatory pathophysiology in biological and preclinical disease models.

1 | Introduction

Neutrophils, the most abundant granulocytic leukocytes in humans, are the principal cellular effectors of the innate immune response [1]. Upon activation by infectious or inflammatory stimuli, these phagocytic cells rapidly migrate to affected tissues and undergo a respiratory burst, during which NADPH oxidase reduces molecular oxygen to superoxide ($O_2^{\bullet-}$), which subsequently dismutates to hydrogen peroxide (H_2O_2) [2, 3]. Myeloperoxidase (MPO), a heme-containing haloperoxidase stored predominantly in the azurophilic granules of neutrophils and, to a lesser extent, in monocytes, is released into phagosomes or the extracellular space upon neutrophil activation [4, 5]. In these compartments, MPO catalyzes the oxidation of physiological halides by H_2O_2, producing predominantly hypochlorous acid (HOCl, pK_a 7.5) from abundant chloride ions (Cl^-) [6]. HOCl is a potent antimicrobial oxidant that halogenates and oxidizes a broad range of biomolecules, including proteins, lipids, and nucleic acids [7, 8]. Although tightly regulated MPO activity is essential for host defense, excessive or dysregulated MPO activity causes substantial oxidative tissue damage [9, 10]. Elevated MPO activity has been implicated in diverse pathologies,

This is an open access article under the terms of the Creative Commons Attribution-NonCommercial-NoDerivs License, which permits use and distribution in any medium, provided the original work is properly cited, the use is non-commercial and no modifications or adaptations are made.
© 2026 The Author(s). *Angewandte Chemie International Edition* published by Wiley-VCH GmbH

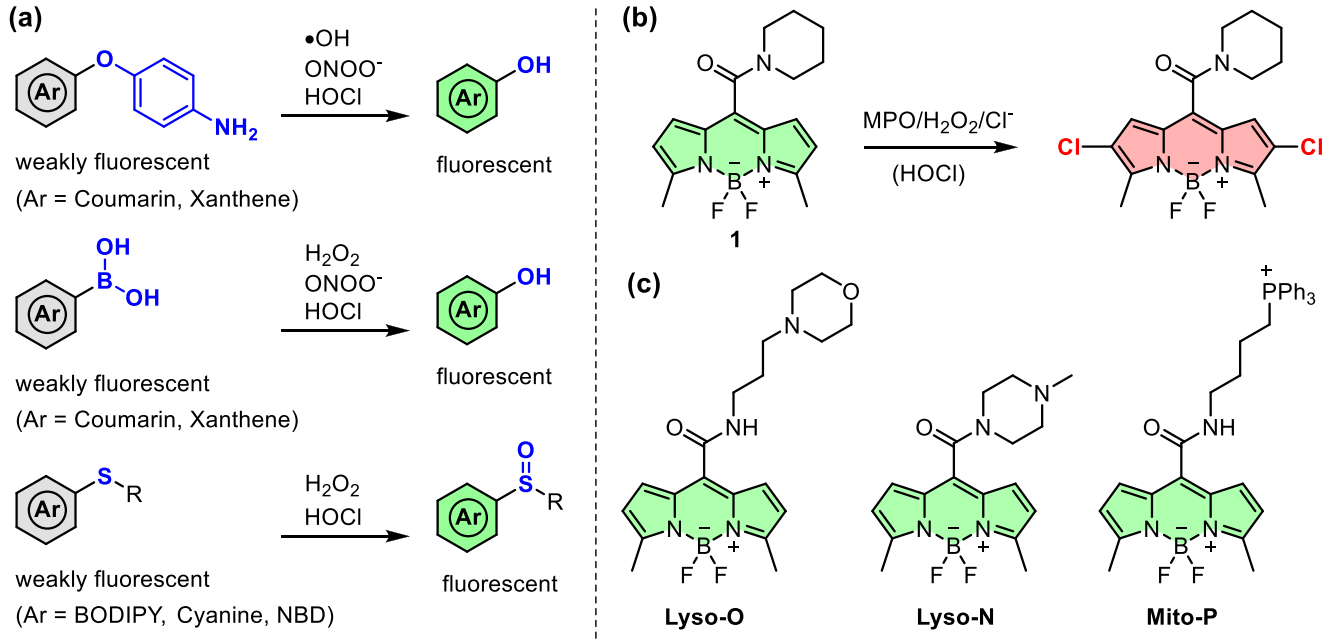


FIGURE 1 | (a) Representative examples of previously reported HOCl-responsive fluorescent probes and their corresponding oxidation products. (b) The chlorination-driven *meso*-carboxamide BODIPY platform **1** developed in this work for selective, fluorescent detection of MPO-derived HOCl. (c) Chemical structures of analogues (**Lyso-O**, **Lyso-N**, and **Mito-P**).

including atherosclerosis, myocardial infarction, acute coronary syndromes, rheumatoid arthritis, chronic kidney disease, pulmonary inflammation, neurodegenerative disorders, and multiple cancers, where it is often associated with poor prognosis [11–20]. MPO is therefore recognized as both a diagnostic biomarker and a therapeutic target [21, 22], as exemplified by the clinical development of MPO inhibitors such as AZD4831 for heart failure [23]. Accurate and real-time monitoring of MPO activity and its major product, HOCl, is thus important for elucidating pathological mechanisms and guiding MPO-targeted therapeutic strategies.

Current analytical methods remain limited for robust assessment of MPO activity in biological systems. Traditional colorimetric or fluorometric assays based on general peroxidase substrates (e.g., TMB [24], ABTS [25], *o*-dianisidine [26] for colorimetry, and Amplex Red [27] for fluorescence) lack specificity and frequently overestimate MPO activity because of cross-reactivity with other heme peroxidases. Enzyme-linked immunosorbent assays (ELISAs), although sensitive, quantify total MPO protein rather than enzymatic activity [28, 29]. By contrast, LC-MS/MS quantification of chlorination biomarkers such as 3-chlorotyrosine (3-Cl-Tyr) provides high specificity and is widely used as an in vivo benchmark of MPO-mediated chlorination, but its destructive and labor-intensive workflow is incompatible with real-time or spatially resolved analysis [30].

Fluorescent probes provide a more convenient approach to HOCl detection, but most reported systems rely on nonspecific oxidative activation mechanisms, including chalcogenide (S/Se/Te) oxidation [31–35], oxidative C═C cleavage [36, 37], boronate oxidation [38, 39], *p*-methoxyphenol oxidation [40], and oxidative cleavage of aminophenyl ethers [41, 42], all of which can also be triggered by competing reactive oxygen and nitrogen species (ROS/RNS), such as H_2O_2, ·OH, and $ONOO^-$ (Figure 1a). Consequently, these probes often produce mixed oxidative readouts and frequently exhibit slow response kinetics or poor performance in complex physiological environments. Moreover, although numerous HOCl-responsive fluorescent probes have been reported [43–47], only a limited subset has been applied to the detection of MPO-derived HOCl (Table S2), and even fewer have demonstrated robust utility across quantitative biochemical MPO assays, cellular imaging, and in vivo inflammatory models.

In principle, electrophilic chlorination can provide a far more selective chemical signature of MPO-derived HOCl, as few endogenous oxidants generate chlorinated organic products. Classical biomarkers such as 3-Cl-Tyr illustrate the inherent selectivity of chlorination chemistry [30], but translating this reaction into a useful fluorescence-based sensing platform remains challenging. HOCl-mediated conversion of dihydroethidine (HE) to 2-chloroethidium is relatively MPO-specific, yet the chlorinated product is only weakly fluorescent and spectrally overlaps with other HE-derived oxidation products, necessitating mass spectrometric analysis [48]. More broadly, although halogenation has been widely used to modulate fluorophore photophysics, including BODIPY dyes for spectral tuning and photosensitizer design [49–52], such transformations often cause only minor spectral shifts or substantial fluorescence quenching in common fluorophore scaffolds, thereby limiting analytical sensitivity and utility in live-cell or in vivo imaging. Early studies using xanthene dyes, including fluorescein and related derivatives, confirmed that HOCl can chlorinate these scaffolds, but the resulting photophysical changes were analytically insufficient, either because the spectral shifts were too small to be practically useful [50] or because chlorination caused severe fluorescence quenching [49, 51]. Thus, the key challenge is not simply achieving fluorophore chlorination, but converting MPO-derived chlorination into a

15213773, 2026, 45, Downloaded from https://onlinelibrary.wiley.com/doi/10.1002/anie.9709775 by Chung-Ang University, Wiley Online Library on [03/11/2026]. See the Terms and Conditions (https://onlinelibrary.wiley.com/terms-and-conditions) on Wiley Online Library for rules of use; OA articles are governed by the applicable Creative Commons License

selective fluorescence response that retains bright emission and provides resolvable spectral shifts.

To address this challenge, we developed a chlorination-driven fluorescent sensing platform based on a *meso*-carboxamide-substituted-3,5-dimethyl BODIPY scaffold (Figure 1b,c). Unlike conventional HOCl probes based largely on nonspecific oxidative activation and prior BODIPY halogenation studies focused mainly on photophysical tuning or photosensitization, this platform uses MPO-derived HOCl chlorination as the fluorescence-reporting reaction itself. Probe **1**, a piperidine-functionalized *meso*-carboxamide-BODIPY, undergoes rapid electrophilic halogenation at the 2,6-positions to yield chlorinated products **2** and **3**, which retain high quantum yields while exhibiting distinct bathochromic shifts of ca. 40 nm. This unusual combination of efficient chlorination, strong fluorescence retention, and clear spectral separation enables highly selective detection of MPO activity through MPO-derived HOCl with minimal interference from other ROS/RNS. Leveraging the synthetic modularity of the *meso*-carboxamide position, this platform was further expanded to organelle-targeted variants through amide conjugation. Across this probe series, MPO and MPO-derived HOCl were detected with high selectivity, enabling quantitative enzyme assays, visualization of exogenous and endogenous MPO activity in cells, discrimination between cancer and normal cells on the basis of oxidative stress-associated redox differences, and noninvasive imaging of MPO-driven inflammation in a mouse model of atopic dermatitis.

2 | Results and Discussion

2.1 | Synthesis of Probes and Photophysical Properties

MPO-responsive probe **1** was synthesized as outlined in Scheme S1. To validate the proposed sensing mechanism of electrophilic chlorination by HOCl generated through the MPO/H_2O_2/Cl^- system, the predicted mono- and di-chlorinated products **2** and **3** were independently prepared (Scheme S1). Analogues (**Lyso-O**, **Lyso-N**, and **Mito-P**) were obtained by incorporating lysosome-targeting morpholine [43, 53] (**Lyso-O**) or piperazine [54] (**Lyso-N**) units, or a mitochondria-targeting triphenylphosphonium moiety [43, 53] (**Mito-P**) at the *meso*-carboxamide position (Scheme S1-S2). All compounds were fully characterized by ^{1}H NMR, ^{13}C NMR, and high-resolution mass spectrometry (HR-MS).

Probe **1** was selected as the representative compound for photophysical characterization. Its properties, along with those of the chlorinated derivatives (**2** and **3**) were measured in acetate buffer (100 mM, pH 5.0, 1% EtOH), conditions chosen to mimic standard MPO assay environments (Table S1). In this medium, probe **1** exhibited absorption and emission maxima ($\lambda_{abs}/\lambda_{em}$) at 516/536 nm with a high fluorescence quantum yield ($\Phi_{FL} = 0.96$), closely matching values obtained in ethanol ($\lambda_{abs}/\lambda_{em}$ = 515/535 nm, $\Phi_{FL} = 0.96$) (Figure 2b,c and Figure S1). This minimal solvent dependence indicates that probe **1** exhibits robust and stable photophysical behavior across both aqueous and organic media. Relative to probe **1**, the chlorinated products **2** and **3** displayed distinct bathochromic shifts: compound **2** exhibited $\lambda_{abs}/\lambda_{em}$ at

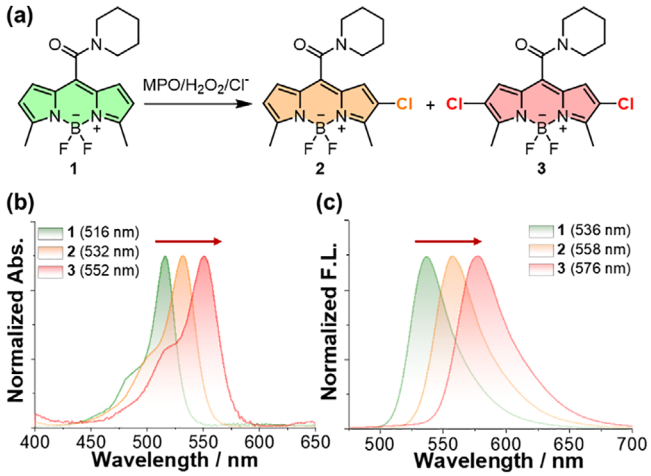


FIGURE 2 | (a) Proposed sensing scheme for MPO activity based on electrophilic chlorination of probe **1**. (b, c) Normalized absorbance (b) and fluorescence (c) spectra of **1**, **2**, and **3** in acetate buffer (100 mM, pH 5.0, 1% EtOH, 25°C). Emission spectra were recorded with excitation at 460 nm for **1** and 500 nm for **2** and **3**.

532/558 nm ($\Phi_{FL} = 0.83$) and compound **3** showed $\lambda_{abs}/\lambda_{em}$ at 552/576 nm ($\Phi_{FL} = 0.74$) (Figure 2). Similar values were observed in ethanol ($\lambda_{abs}/\lambda_{em}$ = 529/555 nm, $\Phi_{FL} = 0.94$ for **2**; 548/573 nm, $\Phi_{FL} = 0.84$ for **3**; Figures S2–S5), confirming solvent-independent spectral behavior. Importantly, the substantial spectral separation between probe **1** and its chlorinated products, combined with consistently high quantum yields, supports dual-mode (chromogenic and fluorescent) detection of MPO-generated HOCl. The fluorescence quantum yield of the dichlorinated product **3** remains high ($\Phi_{FL} = 0.74$ in the assay buffer). This is notable because 2,6-dihalogenated BODIPYs are widely used as triplet photosensitizers. Compared to bromine and iodine, chlorine substitution is only accompanied by a weak heavy-atom effect, as evidenced in the literature for 2,6-dihalogenated BODIPYs [52]. This photophysical profile stands in marked contrast to previously reported chlorination-based probes built on xanthene scaffolds, which suffered from either negligible spectral shifts or severe fluorescence quenching upon halogenation [49, 51].

2.2 | HOCl Sensing in Aqueous Buffer Solution

Because MPO generates HOCl from H_2O_2 and Cl^-, the direct HOCl-response of probe **1** before evaluating its performance in MPO assays was first assessed. Addition of HOCl (100 μM) to **1** (5 μM) in acetate buffer (100 mM, pH 5.0, 1% EtOH, 37°C) induced rapid (≤ 5 min) and pronounced spectral changes (Figure 3). The original absorption and fluorescence bands of **1** ($\lambda_{abs}/\lambda_{em}$ = 516/536 nm) decreased, accompanied by the emergence of red-shifted features at λ_{abs} = 552 nm and λ_{em} = 576 nm, consistent with formation of the di-chlorinated product **3** (Figure 3a,b). Concomitantly, the solution color changed from pink to purple under ambient light, and the fluorescence shifted from green to orange under 365 nm illumination (Figure 3a,b, insets), enabling straightforward naked-eye detection.

Time-course studies confirmed that both absorbance and fluorescence changes proceeded rapidly and reached completion

15213773, 2026, 45, Downloaded from https://onlinelibrary.wiley.com/doi/10.1002/anie.9709775 by Chung-Ang University, Wiley Online Library on [03/11/2026]. See the Terms and Conditions (https://onlinelibrary.wiley.com/terms-and-conditions) on Wiley Online Library for rules of use; OA articles are governed by the applicable Creative Commons License

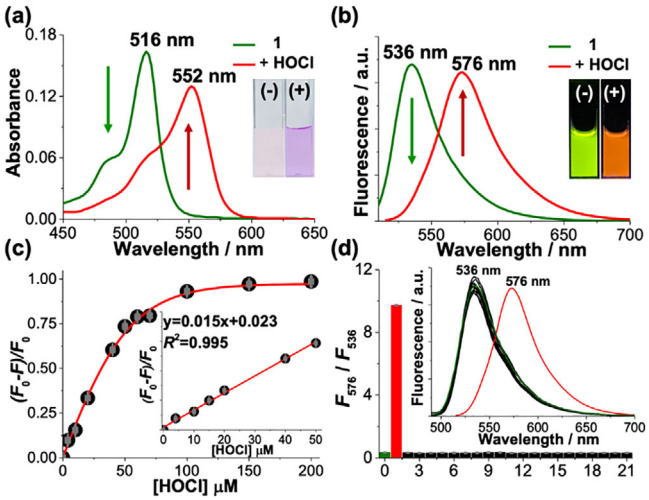


FIGURE 3 | UV/vis absorption (a) and fluorescence emission (b) spectra of probe **1** (5 μM) before (green) and after (red) treatment with HOCl (100 μM) in acetate buffer (100 mM, pH 5.0, 1% EtOH, 37°C). λ_{ex} = 460 nm (green) and 500 nm (red). Incubation: 5 min. Insets: Photos of **1** (10 μM) before (−) and after (+) HOCl addition under ambient light (a) and UV light (365 nm, b). (c) Fluorescence response $[(F_0\text{-}F)/F_0]$ at 536 nm versus [HOCl] (0–200 μM). Incubation: 5 min. F_0 and F represent fluorescence intensities at 536 nm in the absence and presence of HOCl, respectively (λ_{ex} = 460 nm). Inset: A linear relationship between fluorescence intensity $[(F_0\text{-}F)/F_0]$ at 536 nm vs. [HOCl] (0–50 μM). (d) Selectivity of **1** (5 μM) toward various analytes, expressed as the F_{576}/F_{536} ratio. Analytes: (0) **1** only as a control, (1) HOCl (100 μM) (2) glucose, (3) His, (4) Lys, (5) Gly, (6) Trp, (7) Cys, (8) GSH (reduced), (9) glutathione peroxidase (GPx), (10) horseradish peroxidase (HRP), (11) trypsin, (12) lysozyme, (13) lipase, (14) esterase, (15) BSA, (16) $O_2^{\bullet-}$, (17) H_2O_2, (18) ^{t}BuOOH, (19) $ONOO^-$, (20) •OH, and (21) •O^{t}Bu. Conditions: [Analytes 2–15] = 1 mg/mL; [Analytes 16–21] = 100 μM. Incubation = 5 min for HOCl; 12 h for others. λ_{ex} = 460 nm. Inset: Emission spectra of **1** treated with HOCl (red, λ_{ex} = 500 nm) and other analytes (black, λ_{ex} = 460 nm).

within 30 min (Figure S6). Kinetic analysis under pseudo-first-order conditions yielded second-order rate constants of 8.7×10^2 $M^{-1}\cdot s^{-1}$ for the monochlorination of probe **1** to give **2**, and 8.0×10^1 $M^{-1}\cdot s^{-1}$ for the subsequent dichlorination of **2** to give **3** (Figure S7), confirming that the initial chlorination step proceeds approximately 10-fold faster than the second, consistent with the progressive accumulation of **3** at higher HOCl concentrations and the sequential **1→2→3** pathway supported by time-dependent HPLC analysis (Figure S15). HOCl-induced spectral changes were concentration-dependent (Figure 3c and Figures S8 and S9), yielding linear calibration curves suitable for quantitative analysis. Excellent linearity was observed for both absorbance at 552 nm (R^2 = 0.983, Figure S10) and for the fluorescence response $[(F_0\text{–}F)/F_0]$ at 536 nm (R^2 = 0.995, Figure 3c, inset) over 0–50 μM HOCl, with limits of detection (LOD, 3σ/slope) of 0.13 μM (absorbance) and 0.20 μM (fluorescence) (Figure S10). These values are comparable to those of previously reported HOCl probes and are well suited for detecting physiologically and pathophysiologically relevant HOCl concentrations encountered in inflammatory microenvironments, which typically fall in the micromolar range (20–400 μM over 1 h, reaching up to low millimolar levels at dense inflammatory loci) [43–47]. Probe **1** also exhibited excellent baseline stability, showing no significant spectral changes over 10 h under assay conditions (Figure S11), and remained chemically stable across pH 3–8 (Figure S12). The optical response was most pronounced under mildly acidic conditions (pH ≤ 6.5) (Figures S13 and S14), consistent with HOCl (pK_a = 7.5) being the dominant chlorinating species in this range. Accordingly, pH 5.0 was selected for all subsequent cell-free and ex vivo assays to maximize HOCl-mediated chlorination efficiency and enable direct comparison across experiments.

Selectivity studies confirmed that probe **1** is remarkably specific to HOCl (Figure 3d). Negligible spectral changes were observed upon exposure to a broad panel of other ROS/RNS including superoxide ($O_2^{\bullet-}$), hydrogen peroxide (H_2O_2), *tert*-butyl hydroperoxide (^{t}BuOOH), peroxynitrite ($ONOO^-$), hydroxyl radical (•OH), and *tert*-butoxy radicals (•O^{t}Bu), as well as potential biological interferents such as amino acids/biothiols (His, Lys, Gly, Trp, Cys, GSH, and HCy), glucose, bovine serum albumin, and common hydrolytic enzymes (trypsin, lysozyme, lipase, and esterase), even after 12 h of incubation. HPLC-MS analysis confirmed compound **3** as the major reaction product (Figures S15 and S16), consistent with a chlorination-driven sensing mechanism. In contrast, widely used HOCl-responsive probes FLBA (fluorescein-based boronic acid) [55] and APF (3'-(*p*-aminophenyl)fluorescein) [41, 42] exhibited significant cross-reactivity with $ONOO^-$, H_2O_2, and/or •OH (Figures S17–S20). This comparison highlights the superior selectivity of probe **1** for HOCl over competing ROS/RNS.

2.3 | MPO Activity Assays in Buffer Solution

Building upon the validated HOCl response of probe **1**, we next evaluated its performance for the quantitative detection of MPO. Optimized assay conditions were identified as acetate buffer (100 mM, pH 5.0, 1% EtOH) containing 100 mM KCl and 50 μM H_2O_2 at 37°C (Figures S21–S23). Under these conditions, treatment of probe **1** (5 μM) with MPO generated the characteristic absorption and emission bands of dichlorinated product **3** ($\lambda_{abs}/\lambda_{em}$ = 552/576 nm), accompanied by a decrease in the parent probe signals at 516/536 nm (Figures S24 and S25). HPLC–MS analysis confirmed **3** as the primary product (Figure 4a-3), consistent with MPO-driven HOCl formation followed by electrophilic chlorination.

The absorbance at 552 nm and the fluorescence response $[(F_0\text{-}F)/F_0]$ at 536 nm increased progressively with MPO concentration (0–1000 ng/mL) and incubation time (0–33 min) (Figure S26). Probe **1** exhibited excellent linearity across this entire range for both readouts (absorbance: R^2 = 0.993; fluorescence: R^2 = 0.988, Figure 4b). This range encompasses physiologically relevant MPO concentrations from healthy baselines (~20–60 ng/mL) to those associated with inflammatory disease (typically ~60-300 ng/mL, up to ~1000 ng/mL) [28, 29]. LODs were 0.13 ng/mL (absorbance, Figure S27) and 0.25 ng/mL (fluorescence, Figure S28), outperforming many current MPO assay probes (Table S2). Consistent with the pH-dependent HOCl response, MPO-induced spectral shifts were maximal at pH 5.0, with substantial responses still observed at pH 5.5–6.5 (Figure S23). Control experiments confirmed that the response required the simultaneous presence of MPO, H_2O_2, and Cl^- (entry 2 in Figure 4c and Figure S29); omission of any component abolished spectral shifts.

15213773, 2026, 45, Downloaded from https://onlinelibrary.wiley.com/doi/10.1002/anie.9709775 by Chung-Ang University, Wiley Online Library on [03/11/2026]. See the Terms and Conditions (https://onlinelibrary.wiley.com/terms-and-conditions) on Wiley Online Library for rules of use; OA articles are governed by the applicable Creative Commons License

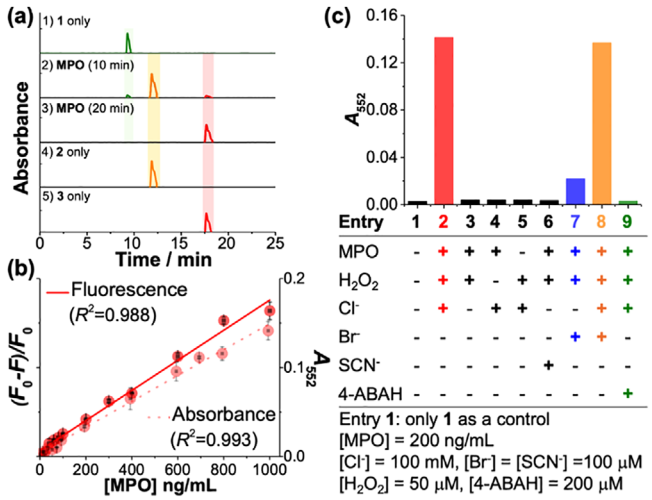


FIGURE 4 | (a) HPLC monitoring of the reaction of **1** (5 μM) in the absence (1) and presence of MPO (150 ng/mL) after 10 min (2) and 20 min (3), showing formation of mono- and di-chlorinated products **2** (4) and **3** (5). Conditions: acetate buffer (100 mM, pH 5.0, 1% EtOH) containing 100 mM KCl and 50 μM H_2O_2 at 37°C. (b) Calibration plots for MPO (0–1000 ng/mL) based on fluorescence response $[(F_0\text{-}F)/F_0]$ at 536 nm (left axis, $R^2 = 0.988$) and absorbance at 552 nm (right axis, $R^2 = 0.993$). Spectra of **1** were recorded 3 min after MPO addition under the conditions above (λ_{ex} = 460 nm). (c) Absorbance at 552 nm of **1** under the indicated assay conditions. Spectra were recorded 20 min after addition of **1** to each solution.

Because SCN^- (20–100 μM in plasma) is a kinetically preferred MPO substrate that can divert enzyme turnover toward HOSCN [6], probe **1** was evaluated under MPO/H_2O_2/SCN^- conditions (100 μM NaSCN; entry 6, Figure 4c and Figure S29). Negligible spectral changes were observed, consistent with HOSCN not undergoing electrophilic aromatic substitution on the BODIPY core. However, competition for MPO by SCN^- may reduce the net HOCl flux and attenuate the probe response in vivo. Treatment with MPO/H_2O_2/Br^- (100 μM KBr, entry 7, Figure 4c and Figure S29) produced a slight decrease in the parent absorption/emission bands, without generating the red-shifted absorption/emission features at 552/576 nm or increasing in F_{576}/F_{536}. Moreover, when Cl^- and Br^- were present together (entry 8, Figure 4c and Figure S29), the response closely matched that observed with Cl^- alone (entry 2). Therefore, at physiologically relevant concentrations, Br^- does not substantially interfere with Cl^- and MPO-derived HOBr does not induce a confounding ratiometric signal under assay conditions. Specificity was further supported by inhibition studies: the absorbance increase at 552 nm was dose-dependently suppressed by the MPO inhibitor 4-aminobenzoic acid hydrazide [56] (4-ABAH: IC_{50} = 42.0 ± 1.9 nM, entry 9 in Figure 4c and Figure S31) and by the HOCl scavenger *N*-acetylcysteine (NAC: IC_{50} = 2.14 μM, Figure S32). The IC_{50} value for 4-ABAH agrees well with reported values [57], confirming the suitability of **1** for quantitative MPO assays and potential high-throughput inhibitor screening. Notably, probe **1** also exhibited excellent selectivity, producing the characteristic red-shifted spectral response exclusively with MPO and remaining unresponsive to other peroxidases, including glutathione peroxidase, horseradish peroxidase, and eosinophil peroxidase (Figure S30). Collectively, these results establish an electrophilic chlorination-based platform as a rapid, sensitive, and highly selective dual-mode (chromogenic and fluorescent) system for the detection of MPO activity and MPO-derived HOCl.

2.4 | Fluorescence Imaging of Exogenous and Endogenous MPO-Derived HOCl in Cells

To enable subcellular visualization of MPO-derived HOCl, analogues of probe **1** were prepared by appending established targeting motifs at the *meso*-carboxamide position: morpholine (**Lyso-O**) and piperazine (**Lyso-N**) for lysosomes, and triphenylphosphonium (**Mito-P**) for mitochondria. Lysosomal targeting was prioritized because MPO is predominantly localized in azurophilic, lysosome-like granules in neutrophils and internalized MPO in macrophages is trafficked to endolysosomal vesicles, the primary intracellular sites of MPO activity and HOCl generation [4, 5]. Enrichment of the probes in these compartments was therefore expected to maximize access to MPO-derived HOCl. **Mito-P** was included based on emerging evidence that MPO is not exclusively confined to lysosomes but is also present in the mitochondria of macrophages [58, 59]. Furthermore, mitochondria are particularly vulnerable to HOCl-mediated oxidative damage during inflammatory responses [60]. The three derivatives preserved the characteristic MPO/Cl^-/H_2O_2-triggered spectral response of probe **1** (Figures S33–S47), indicating that installation of the targeting groups did not perturb the sensing mechanism. Colocalization studies with commercial organelle trackers indicated preferential enrichment in the intended subcellular compartments, rather than exclusive localization, with Pearson correlation coefficients of 0.56 for **Lyso-O**, 0.69 for **Lyso-N**, and 0.54 for **Mito-P** (Figures S49 and S50). By comparison, probe **1** showed weak colocalization with lysosomes (0.48) and mitochondria (0.38), consistent with its non-targeted intracellular distribution (Figures S49 and S50). The cytotoxicity of probe **1** and the targeted derivatives (**Lyso-O**, **Lyso-N**, and **Mito-P**) was evaluated in three representative cell lines: HL-60 (human promyelocytic leukemia, high MPO expression), K562 (human chronic myelogenous leukemia, low MPO expression), and RAW 264.7 (murine macrophages, low MPO expression) [61–63]. All probes maintained cell viability above 88% at concentrations up to 20 μM in all three cell lines (Figure S48), confirming their suitability for cellular imaging applications.

We first assessed whether the probes could visualize, in cells, exogenous generation of MPO-derived HOCl. RAW 264.7 macrophages, which exhibit very low basal MPO activity [61–63], were treated extracellularly with an MPO/Cl^-/H_2O_2 system (100 mM acetate buffer, pH 5.0, 1% EtOH) and analyzed by confocal fluorescence microscopy (Figure 5a). Cells incubated with probe **1** alone exhibited predominantly green fluorescence (1), consistent with the unreacted form of the probe. In contrast, treatment with the complete MPO/Cl^-/H_2O_2 system induced a pronounced green-to-red fluorescence transition, characterized by decreased emission in the green channel (Figure 5a-6; Ex/Em = 488/520–540 nm) and markedly increased emission in the red channel (Figure 5a-7; Ex/Em = 488/570–590 nm), reflecting conversion of the probe to its chlorinated products. Quantitative analysis showed a 6–7-fold increase in the $F_{Red/Green}$ ratio across all probe variants, including **Lyso-O**, **Lyso-N**, and **Mito-P**, indicating that incorporation of targeting motifs does

15213773, 2026, 45, Downloaded from https://onlinelibrary.wiley.com/doi/10.1002/anie.9709775 by Chung-Ang University, Wiley Online Library on [03/11/2026]. See the Terms and Conditions (https://onlinelibrary.wiley.com/terms-and-conditions) on Wiley Online Library for rules of use; OA articles are governed by the applicable Creative Commons License

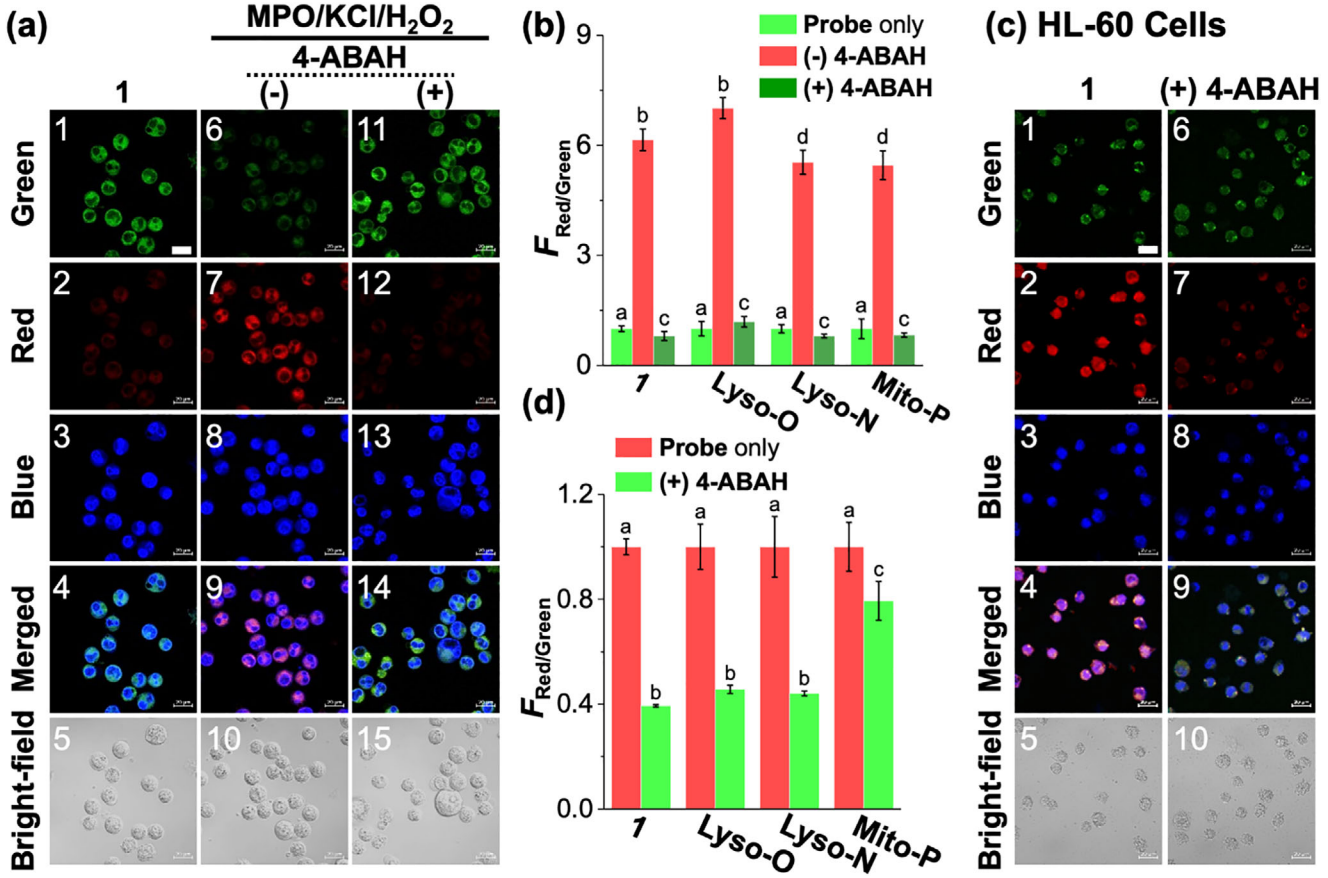


FIGURE 5 | (a) Confocal fluorescence images of RAW 264.7 macrophages loaded with probe **1** (5 μM, 30 min) (1–5) and then treated extracellularly with KCl (100 mM), H_2O_2 (50 μM), and MPO (100 ng/mL) in the absence (6–10) or presence (11–15) of the MPO inhibitor 4-ABAH (200 μM, 30 min). Conditions: acetate buffer (100 mM, pH 5.0, 1% EtOH). Following probe loading and the indicated treatments, cells were synchronously fixed with 4% PFA to terminate the MPO-dependent sensing reaction prior to confocal imaging, and counterstained with DAPI for nuclear visualization. (b) Quantification of the fluorescence intensity ratio ($F_{Red/Green}$) in RAW 264.7 cells treated with probe **1**, **Lyso-O**, **Lyso-N**, or **Mito-P** under the indicated conditions. (c) Confocal fluorescence images of HL-60 cells loaded with probe **1** (5 μM, 30 min) under basal conditions (1–5) or after pre-treatment with 4-ABAH (200 μM, 30 min) (6–10). (d) Quantification of the fluorescence intensity ratio ($F_{Red/Green}$) in HL-60 cells treated with probe **1**, **Lyso-O**, **Lyso-N**, or **Mito-P** under the indicated conditions. Cells were co-stained with DAPI for nuclear visualization. From top to bottom: green channel (Ex/Em = 488/520–540 nm), red channel (Ex/Em = 488/570–590 nm), blue channel (Ex/Em = 405/450–480 nm), merged images, and bright-field images. Scale bar: 20 μm. Data are presented as mean ± SEM ($n = 9$). Different letters denote statistically significant differences ($p < 0.05$). Data in (b) and (d) were normalized to the fluorescence ratio from cells treated with probe only.

not compromise sensing performance (Figure 5b and Figure S51). The chlorinated products **2** and **3** showed neither significant $^1O_2$ generation (Figures S67–S69) nor detectable photobleaching (Figures S62–S66) under laser illumination. Probe-derived ROS generation through photosensitization and self-sensitized photodegradation therefore does not bias the fluorescence readout in cellular imaging.

Importantly, the fluorescence response was strongly suppressed by co-incubation with the MPO inhibitor 4-ABAH (200 μM) (Figure 5a-11,12; Figure 5b), restoring signal close to the probe-only condition. These results confirm that the observed fluorescence switching arises from MPO-dependent HOCl generation rather than nonspecific probe activation. Notably, probe-treated cells showed weak basal red fluorescence even in the absence of exogenous MPO stimulation (Figure 5a-2), whereas red-channel emission was further reduced in the presence of 4-ABAH (Figure 5a-12). This result suggests that probe **1** is sufficiently sensitive to detect trace endogenous MPO-derived HOCl production, even in cells with minimal MPO expression. Similar fluorescence responses were also observed in K562 cells (Figure S52), further supporting the general applicability of this platform across distinct low-MPO cell types.

Having established robust detection of exogenous MPO activity using the MPO/Cl^-/H_2O_2 system, we next assessed whether the probes could detect physiologically generated HOCl in HL-60 cells, a human promyelocytic leukemia cell line known to express high levels of endogenous MPO [61–63]. Cells were imaged under basal conditions and after pre-treatment with the MPO inhibitor 4-aminobenzoic acid hydrazide (4-ABAH, 200 μM, 30 min) (Figure 5c,d). Under basal conditions, all probes produced measurable red fluorescence in HL-60 cells (Figure 5c-2; Figure S54), consistent with constitutive endogenous HOCl generation. Pre-treatment with 4-ABAH markedly suppressed the red fluorescence signal (Figure 5c-7; Figure S54), resulting in an approximately 54%–61% decrease in the $F_{Red/Green}$ ratio for probe **1**, **Lyso-O**, and **Lyso-N** (Figure 5d). These results indicate that the

15213773, 2026, 45, Downloaded from https://onlinelibrary.wiley.com/doi/10.1002/anie.9709775 by Chung-Ang University, Wiley Online Library on [03/11/2026]. See the Terms and Conditions (https://onlinelibrary.wiley.com/terms-and-conditions) on Wiley Online Library for rules of use; OA articles are governed by the applicable Creative Commons License

observed fluorescence signals arise predominantly from MPO-dependent intracellular HOCl. By contrast, **Mito-P** showed only a modest reduction in $F_{Red/Green}$ upon 4-ABAH pre-treatment (ca. 21%; Figure 5d and Figure S54). This weaker inhibitor response may reflect its mitochondrial localization.

Notably, probe **1** exhibited substantially stronger basal red fluorescence in HL-60 cells than in K562 or RAW 264.7 cells, both of which express low MPO levels (Figure S56), consistent with the higher endogenous HOCl flux associated with elevated MPO expression in HL-60 cells. The ability to distinguish high- and low-MPO cell lines indicates that these probes not only detect endogenous HOCl but also report differences in MPO activity across distinct cellular contexts. Collectively, these results establish this probe platform as a sensitive and selective tool for detecting both exogenous and endogenous MPO-catalyzed HOCl in cells.

2.5 | Oxidative Stress–Based Discrimination Between Cancer and Normal Cells

Cancer cells often exhibit elevated oxidative stress arising from altered metabolism and mitochondrial dysfunction, leading to higher basal H_2O_2 levels than those in normal cells [64, 65]. Because H_2O_2 is a key substrate for MPO-catalyzed HOCl generation, we investigated whether the probes could discriminate cancer versus normal cells on the basis of their differential redox states. In the presence of exogenous MPO/Cl^-, lysates from human breast cancer cells (MCF7) and lung cancer cells (A549) showed 1.5–1.7-fold higher $F_{Red/Green}$ ratios than those from their corresponding normal counterparts, MCF10A and MRC5, respectively (A549 vs. MRC5; MCF7 vs. MCF10A, Figure 6a and Figure S58). This difference is consistent with the higher endogenous H_2O_2 levels in cancer cells, which promote HOCl production under MPO-supplemented conditions. To further accentuate metabolic differences, cells were pre-treated with antimycin A (AntA), a mitochondrial complex III inhibitor that induces mitochondrial dysfunction and markedly increases intracellular H_2O_2 production [66]. Following AntA treatment, cancer cell lysates exhibited substantially higher $F_{Red/Green}$ ratios than their corresponding normal cell lysates, with increases of approximately 4-fold for the MCF7/MCF10A pair and 6–7-fold for the A549/MRC5 pair (Figure 6a and Figure S58). Similar trends were observed across all probe variants, demonstrating the robustness of the probe platform for distinguishing cancer from normal cells on the basis of oxidative stress-associated HOCl generation. We note that this discrimination experiment relies on exogenous MPO/Cl^- supplementation and is therefore not a direct diagnostic assay for endogenous MPO activity. Rather, the probe reports differential H_2O_2-dependent HOCl generation between cancer and normal cell lysates under standardized MPO-supplemented conditions. It may be applicable to ex vivo redox profiling, rather than direct in vivo cancer diagnosis.

2.6 | Cellular and Ex Vivo Detection of Inflammatory Responses

To assess probe performance under inflammatory conditions, RAW 264.7 macrophages were stimulated with lipopolysaccharide (LPS) that induces pro-inflammatory and oxidative responses. LPS-treated cells showed substantially higher red fluorescence and elevated $F_{Red/Green}$ ratios (1.4–1.8) than untreated controls (Figure 6b and Figure S53), indicating increased HOCl levels during inflammatory activation. This enhancement in $F_{Red/Green}$ is consistent with LPS-induced oxidative signaling, which promotes a respiratory burst and increases intracellular H_2O_2 production [67, 68], thereby facilitating HOCl formation from endogenous MPO activity or MPO internalized under inflammatory conditions. While cell-free assays, ex vivo experiments, and cellular imaging of exogenous MPO-derived HOCl were conducted at pH 5.0, endogenous cellular imaging was performed under physiological culture conditions, where HOCl and OCl^- coexist (~1:1 at pH 7.4). Importantly, MPO-derived chlorination in biological systems typically occurs within mildly acidic microenvironments — including lysosomes (pH 4.5–5.0), phagosomes/phagolysosomes (pH 5–6.5), and locally acidic inflammatory or cancerous tissues (pH 4.0–6.5) — rather than solely at bulk extracellular pH [69–72]. The fluorescence responses are therefore best interpreted as reporting MPO-associated chlorinating activity within local organellar or inflammatory microenvironments, where HOCl/OCl^- speciation is governed by the local rather than bulk extracellular pH.

To further evaluate probe performance in primary immune cells under inflammatory conditions, the probes were applied to granulocytes isolated from LPS-treated mice. Plasma/granulocyte mixtures from LPS-treated mice exhibited 1.6–1.9-fold higher $F_{Red/Green}$ ratios than those from untreated control mice (Figure 6c), confirming that the probes can detect inflammation-associated HOCl production in primary immune cells obtained from an in vivo inflammatory model. These cellular and ex vivo results demonstrate that the probes sensitively capture HOCl elevations associated with inflammatory activation, supporting their utility for monitoring MPO-derived HOCl production during active immune responses.

2.7 | In Vivo Visualization of Inflammation in an Atopic Dermatitis Mouse Model

To extend these findings in vivo, the probe series was evaluated in a 2,4-dinitrochlorobenzene (DNCB)-induced atopic dermatitis (AD) mouse model, a well-established model of chronic skin inflammation [73]. Following tail-vein injection of the probes, clear differences in fluorescence patterns were observed among healthy control and DNCB-treated AD mice. Healthy control animals displayed strong green fluorescence with weak red fluorescence, whereas DNCB-treated AD mice showed the opposite trend, with diminished green fluorescence and markedly enhanced red fluorescence at superficial inflamed dorsal skin sites (Figure 7a). This fluorescence shift resulted in significantly elevated $F_{Red/Green}$ ratios across all probes in the AD group relative to healthy controls: probe **1** (~8-fold), **Mito-P** (~8-fold), **Lyso-N** (~10-fold), and **Lyso-O** (~12-fold) (Figure 7b). 4-ABAH treatment in vivo (40 mg/kg, i.p., once daily during AD induction) markedly suppressed the DNCB-induced elevation in $F_{Red/Green}$ ratios across all probes (Figure 7b), providing pharmacological evidence that the fluorescence response is driven by MPO activity in inflamed skin lesions rather than nonspecific oxidative processes. The probe-dependent differences in $F_{Red/Green}$ ratios likely reflect

15213773, 2026, 45, Downloaded from https://onlinelibrary.wiley.com/doi/10.1002/anie.9709775 by Chung-Ang University, Wiley Online Library on [03/11/2026]. See the Terms and Conditions (https://onlinelibrary.wiley.com/terms-and-conditions) on Wiley Online Library for rules of use; OA articles are governed by the applicable Creative Commons License

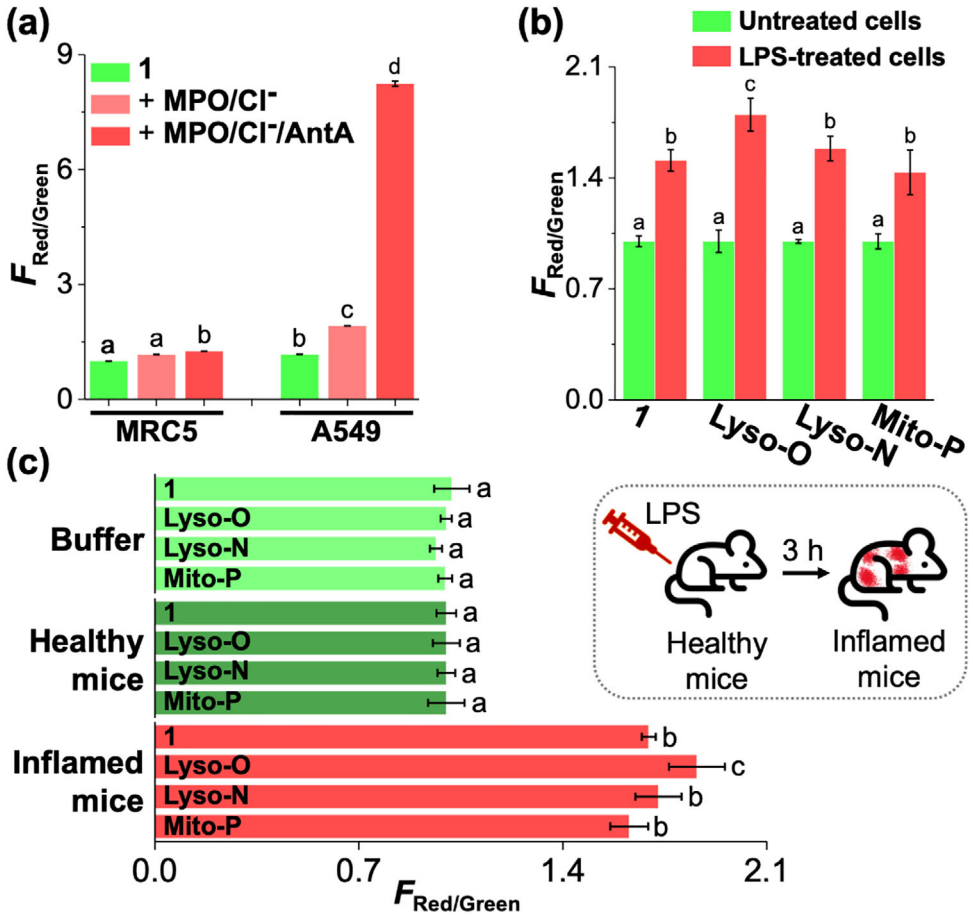


FIGURE 6 | (a) Comparative fluorescence ratios ($F_{Red/Green}$) of probe **1** measured in lysates from normal (MRC5), cancer (A549), and antimycin A (AntA)-treated (red) cells, shown in the absence (green) and presence (pale red and red) of MPO/KCl. Cell lysates were analyzed in acetate buffer (100 mM, pH 5.0) with or without MPO (100 ng/mL)/KCl (100 mM). (b) Relative fluorescence response ($F_{Red/Green}$) in probe (5 μM)-loaded RAW 264.7 macrophages under basal conditions (green) or after stimulation with lipopolysaccharide (LPS, red). (c) Relative fluorescence response ($F_{Red/Green}$) for probe **1**, **Lyso-O**, **Lyso-N**, and **Mito-P** in the absence (pale green) and presence of plasma/granulocyte mixtures isolated from uninflamed healthy (green) or LPS-injected inflamed mice (red). Plasma/granulocyte mixtures were analyzed in acetate buffer (100 mM, pH 5.0). Ratios were normalized to the uninflamed healthy control group. Data are presented as mean ± SEM ($n = 9$). Different letters denote statistically significant differences ($p < 0.05$).

variations in systemic biodistribution and tissue accumulation among the probe variants rather than subcellular organelle targeting per se, and should be interpreted with caution given the small sample size ($n = 3$).

The robust fluorescent response reflects elevated HOCl production at sites of inflammation, likely driven by infiltrating neutrophils and other activated immune cells that release MPO within AD lesions. Successful induction of the AD model was verified by RT-PCR analysis, which showed significant upregulation of AD-associated inflammatory biomarkers, including Nos2, Mmp8, Mmp9, and Ccl27 [74], in DNCB-treated skin (Figure 7c). Notably, 4-ABAH treatment reduced the expression of these inflammatory markers relative to the DNCB-only group (Figure 7c), consistent with suppression of MPO-associated inflammatory activation. Histological analysis by H&E staining further revealed pronounced epidermal and dermal thickening, a hallmark feature of AD, in DNCB-treated mice (Figure 7d), which was attenuated upon 4-ABAH treatment (Figure S60). Fluorescence localization studies demonstrated preferential accumulation of the probes in inflamed AD skin tissue, with minimal signals in healthy skin (Figure 7e), indicating that both strong fluorescent activation and selective tissue localization contribute to the high imaging contrast observed. As an additional line of evidence, MPO enzymatic activity, measured directly in skin tissue lysates using a commercial colorimetric *o*-dianisidine MPO activity assay, was significantly elevated in DNCB-treated AD mice relative to healthy controls and was substantially reduced upon 4-ABAH treatment (Figure S61), corroborating the in vivo imaging results and confirming that the fluorescence signal specifically reflects local MPO-derived HOCl production. Collectively, these results demonstrate that the probe series sensitively detects MPO-mediated HOCl production in an inflammatory skin model, highlighting their potential for non-invasive imaging of inflammatory disorders.

3 | Conclusion

In summary, we have developed a chlorination-driven BODIPY fluorescent platform for the highly selective detection of MPO activity and MPO-derived HOCl based on a *meso*-carboxamide-

15213773, 2026, 45, Downloaded from https://onlinelibrary.wiley.com/doi/10.1002/anie.9709775 by Chung-Ang University, Wiley Online Library on [03/11/2026]. See the Terms and Conditions (https://onlinelibrary.wiley.com/terms-and-conditions) on Wiley Online Library for rules of use; OA articles are governed by the applicable Creative Commons License

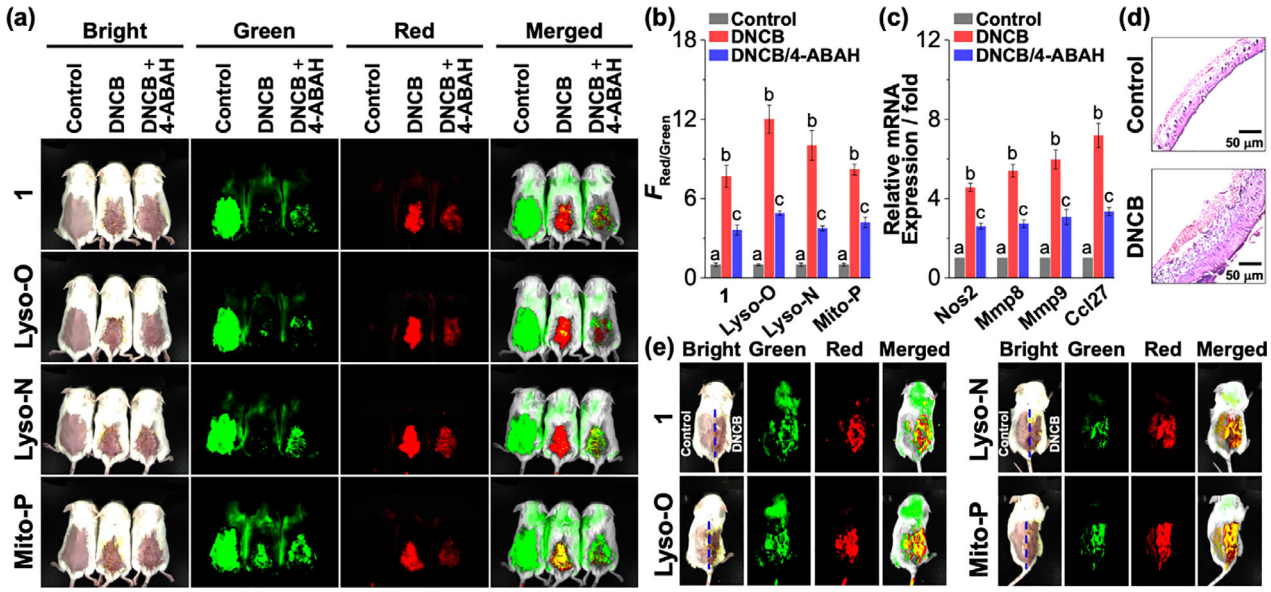


FIGURE 7 | (a) In vivo fluorescence images of healthy control mice, DNCB-induced atopic dermatitis (AD) mice, and DNCB/4-ABAH-treated AD mice after tail-vein injection of probe **1**, **Lyso-O**, **Lyso-N**, or **Mito-P**. AD mice showed decreased green fluorescence and enhanced red fluorescence at superficial inflamed dorsal skin sites relative to healthy controls, whereas 4-ABAH treatment suppressed the DNCB-induced fluorescence response. (b) Quantification of the fluorescence ratio ($F_{Red/Green}$) in healthy control, DNCB-treated, and DNCB/4-ABAH-treated mice for each probe. (c) RT-PCR analysis of AD-associated inflammatory biomarkers (Nos2, Mmp8, Mmp9, and Ccl27) in skin tissues from healthy control, DNCB-treated, and DNCB/4-ABAH-treated mice. (d) H&E-stained skin sections showing epidermal and dermal thickening in DNCB-treated mice. Scale bar: 50 μm. (e) Fluorescence localization images of dorsal skin showing preferential accumulation of the probes in inflamed AD lesions (right side), with minimal signal in healthy skin (left side). Data are presented as mean ± SEM ($n = 3$). Different letters in (b) and (c) denote statistically significant differences ($p < 0.05$).

substituted 3,5-dimethyl BODIPY scaffold. By coupling a chemically well-defined electrophilic chlorination reaction with a fluorophore that retains strong emission after halogenation, this platform overcomes a key limitation of previous chlorination-based systems, namely, weak spectral response or fluorescence quenching. The lead probe exhibits a distinct ca. 40 nm bathochromic shift upon chlorination, enabling sensitive dual-mode detection of MPO-derived HOCl with excellent selectivity over competing ROS/RNS. Importantly, the modular *meso*-carboxamide design also enabled straightforward access to probe derivatives, including **Lyso-O**, **Lyso-N**, and **Mito-P**, without compromising sensing performance. Across this probe series, the strategy proved effective in quantitative MPO assays, cellular imaging of exogenous and endogenous MPO-derived HOCl, discrimination between cancer and normal cells, and detection of inflammation-associated HOCl in cellular, ex vivo, and in vivo models, including a DNCB-induced mouse model of atopic dermatitis. This strategy differs from prior BODIPY halogenation chemistry and conventional HOCl/MPO probes by converting MPO-derived electrophilic chlorination into a selective fluorochromic readout with retained bright emission. Overall, this work establishes electrophilic chlorination as an effective design strategy for MPO-responsive fluorescent probes and expands the molecular toolkit for studying MPO-mediated inflammatory pathways in biological and preclinical disease models.

Author Contributions

Siyoung Cho: methodology, data curation, investigation, writing – review and editing, formal analysis, visualization. **Yongyang Luo**: writing – review and editing, methodology, data curation, formal analysis, investigation, visualization. **Jeehyeon Bae**: writing – review and editing, supervision, funding acquisition, formal analysis. **Youngmi Kim**: writing – original draft, writing – review and editing, supervision, validation, funding acquisition, conceptualization, formal analysis, visualization.

Acknowledgments

This work was supported by the National Research Foundation of Korea (NRF) grants funded by the Korean government (MSIT, No. RS-2025-02216340 to J.B. and No. RS-2024-00353907 to Y.K.).

Conflicts of Interest

The authors declare no conflicts of interest.

Data Availability Statement

The data that supports the findings of this study are available in the Supporting Information of this article.

References

1. G. L. Burn, A. Foti, G. Marsman, D. F. Patel, and A. Zychlinsky, "The Neutrophil," *Immunity* 54 (2021): 1377–1391, https://doi.org/10.1016/j.immuni.2021.06.006.

2. C. C. Winterbourn and A. J. Kettle, "Redox Reactions and Microbial Killing in the Neutrophil Phagosome," *Antioxidants & Redox Signaling* 18 (2013): 642–660, https://doi.org/10.1089/ars.2012.4827.

3. C. C. Winterbourn, A. J. Kettle, and M. B. Hampton, "Reactive Oxygen Species and Neutrophil Function," *Annual Review of Biochemistry* 85 (2016): 765–792, https://doi.org/10.1146/annurev-biochem-060815-014442.

4. S. J. Klebanoff, "Myeloperoxidase: Friend and Foe," *Journal of Leukocyte Biology* 77 (2005): 598–625, https://doi.org/10.1189/jlb.1204697.

15213773, 2026, 45, Downloaded from https://onlinelibrary.wiley.com/doi/10.1002/anie.9709775 by Chung-Ang University, Wiley Online Library on [03/11/2026]. See the Terms and Conditions (https://onlinelibrary.wiley.com/terms-and-conditions) on Wiley Online Library for rules of use; OA articles are governed by the applicable Creative Commons License

5. S. J. Klebanoff, A. J. Kettle, H. Rosen, C. C. Winterbourn, and W. M. Nauseef, "Myeloperoxidase: A Front-Line Defender Against Phagocytosed Microorganisms," *Journal of Leukocyte Biology* 93 (2013): 185–198, https://doi.org/10.1189/jlb.0712349.

6. A. J. Kettle and C. C. Winterbourn, "Myeloperoxidase: A Key Regulator of Neutrophil Oxidant Production," *Redox Report* 3 (1997): 3–15, https://doi.org/10.1080/13510002.1997.11747085.

7. C. C. Winterbourn, "Comparative Reactivities of Various Biological Compounds With Myeloperoxidase-Hydrogen Peroxide-Chloride, and Similarity of Oxidant to Hypochlorite," *Biochimica et Biophysica Acta* 840 (1985): 204–210, https://doi.org/10.1016/0304-4165(85)90120-5.

8. D. I. Pattison and M. J. Davies, "Absolute Rate Constants for the Reaction of Hypochlorous Acid With Protein Side Chains and Peptide Bonds," *Chemical Research in Toxicology* 14 (2001): 1453–1464, https://doi.org/10.1021/tx0155451.

9. A. Strzepa, K. A. Pritchard, and B. N. Dittel, "Myeloperoxidase: A New Player in Autoimmunity," *Cellular Immunology* 317 (2017): 1–8, https://doi.org/10.1016/j.cellimm.2017.05.002.

10. Y. Aratani, "Myeloperoxidase: Its Role for Host Defense, Inflammation, and Neutrophil Function," *Archives of Biochemistry and Biophysics* 640 (2018): 47–52, https://doi.org/10.1016/j.abb.2018.01.004.

11. M.-L. Brennan, M. S. Penn, F. V. Lente, et al., "Prognostic Value of Myeloperoxidase in Patients With Chest Pain," *New England Journal of Medicine* 349 (2003): 1595–1604, https://doi.org/10.1056/NEJMoa035003.

12. O. A. Iakoubova, F. Haji-Sheikhi, J. Z. Louie, et al., "Association of MPO Levels With Cardiometabolic Disease Stratified by Atherosclerotic Cardiovascular Risk and Intensity of Therapy in a Workforce Population," *Scientific Reports* 15 (2025): 12244, https://doi.org/10.1038/s41598-025-89373-7.

13. Y. Chen, F. Zhang, L. Dong, and X. Shu, "Long-Term Prognostic Value of Myeloperoxidase on Acute Coronary Syndrome: A Meta-Analysis," *Archives of Medical Research* 42 (2011): 368–374, https://doi.org/10.1016/j.arcmed.2011.07.004.

14. P. Wu, Y. Zhu, L. Chen, Y. Tian, and H. Xiong, "A Fast-Responsive OFF–ON Near-Infrared-II Fluorescent Probe for In Vivo Detection of Hypochlorous Acid in Rheumatoid Arthritis," *Analytical Chemistry* 93 (2021): 13014–13021, https://doi.org/10.1021/acs.analchem.1c02831.

15. L. Kulander, K. Pauksens, and P. Venge, "Soluble Adhesion Molecules, Cytokines and Cellular Markers in Serum in Patients With Acute Infections," *Scandinavian Journal of Infectious Diseases* 33 (2001): 290–300, https://doi.org/10.1080/003655401300077342.

16. M. O. Breckwoldt, J. W. Chen, L. Stangenberg, et al., "Tracking the Inflammatory Response in Stroke In Vivo by Sensing the Enzyme Myeloperoxidase," *Proceedings of the National Academy of Sciences* 105 (2008): 18584–18589, https://doi.org/10.1073/pnas.0803945105.

17. J. Ke, P. Zhao, J. Li, and Q. Fu, "Visualization of HOCl in the Brains of Alzheimer's Disease Models Using an Easily Available Two-Photon Fluorogenic Probe," *Journal of Materials Chemistry B* 10 (2022): 8744–8749, https://doi.org/10.1039/D2TB01502A.

18. S. Samanta and T. Govindaraju, "Unambiguous Detection of Elevated Levels of Hypochlorous Acid in Double Transgenic AD Mouse Brain," *ACS Chemical Neuroscience* 10 (2019): 4847–4853, https://doi.org/10.1021/acschemneuro.9b00554.

19. E. F. Espejo, M.-D.-M. Guerra, and S. Castellano, "Association Between Serum Myeloperoxidase Enzyme Activity and Parkinson's Disease Status," *npj Parkinson's Disease* 11 (2025): 94, https://doi.org/10.1038/s41531-025-00941-0.

20. B. Pan, H. Ren, X. Lv, et al., "Hypochlorite-Induced Oxidative Stress Elevates the Capability of HDL in Promoting Breast Cancer Metastasis," *Journal of Translational Medicine* 10 (2012): 65, https://doi.org/10.1186/1479-5876-10-65.

21. A. A. Khan, M. A. Alsahli, and A. H. Rahmani, "Myeloperoxidase as an Active Disease Biomarker: Recent Biochemical and Pathological Perspectives," *Medical Sciences* 6 (2018): 33, https://doi.org/10.3390/medsci6020033.

22. K. Jannesar and H. Soraya, "MPO and Its Role in Cancer, Cardiovascular and Neurological Disorders: An Update," *Biochemical and Biophysical Research Communications* 755 (2025): 151578, https://doi.org/10.1016/j.bbrc.2025.151578.

23. T. Inghardt, T. Antonsson, C. Ericsson, et al., "Discovery of AZD4831, a Mechanism-Based Irreversible Inhibitor of Myeloperoxidase, as a Potential Treatment for Heart Failure With Preserved Ejection Fraction," *Journal of Medicinal Chemistry* 65 (2022): 11485–11496, https://doi.org/10.1021/acs.jmedchem.1c02141.

24. P. C. Andrews and N. I. Krinsky, "Quantitative Determination of Myeloperoxidase Using Tetramethylbenzidine as Substrate," *Analytical Biochemistry* 127 (1982): 346–350, https://doi.org/10.1016/0003-2697(82)90185-3.

25. A. Hasmann, E. Wehrschuetz-Sigl, A. Marold, et al., "Analysis of Myeloperoxidase Activity in Wound Fluids as a Marker of Infection," *Annals of Clinical Biochemistry* 50 (2013): 245–254, https://doi.org/10.1258/acb.2011.010249.

26. P. P. Bradley, D. A. Priebat, R. D. Christensen, and G. Rothstein, "Measurement of Cutaneous Inflammation: Estimation of Neutrophil Content With an Enzyme Marker," *Journal of Investigative Dermatology* 78 (1982): 206–209, https://doi.org/10.1111/1523-1747.ep12506462.

27. A. Gomes, E. Fernandes, and J. L. F. C. Lima, "Fluorescence Probes Used for Detection of Reactive Oxygen Species," *Journal of Biochemical and Biophysical Methods* 65 (2005): 45–80, https://doi.org/10.1016/j.jbbm.2005.10.003.

28. M. C. Meuwese, E. S. G. Stroes, S. L. Hazen, et al., "Serum Myeloperoxidase Levels Are Associated With the Future Risk of Coronary Artery Disease in Apparently Healthy Individuals: The EPIC-Norfolk Prospective Population Study," *Journal of the American College of Cardiology* 50 (2007): 159–165, https://doi.org/10.1016/j.jacc.2007.03.033.

29. S. Baldus, C. Heeschen, T. Meinertz, et al., "Myeloperoxidase Serum Levels Predict Risk in Patients With Acute Coronary Syndromes," *Circulation* 108 (2003): 1440–1445, https://doi.org/10.1161/01.CIR.0000090690.67322.51.

30. F. Afshinnia, L. Zeng, J. Byun, et al., Michigan Kidney Translational Core CPROBE Investigator Group, "Myeloperoxidase Levels and Its Product 3-Chlorotyrosine Predict Chronic Kidney Disease Severity and Associated Coronary Artery Disease," *American Journal of Nephrology* 46 (2017): 73–81, https://doi.org/10.1159/000477766.

31. L. Yuan, L. Wang, B. K. Agrawalla, et al., "Development of Targetable Two-Photon Fluorescent Probes to Image Hypochlorous Acid in Mitochondria and Lysosome in Live Cell and Inflamed Mouse Model," *Journal of the American Chemical Society* 137 (2015): 5930–5938, https://doi.org/10.1021/jacs.5b00042.

32. S. V. Mulay, M. Choi, Y. J. Jang, Y. Kim, S. Jon, and D. G. Churchill, "Enhanced Fluorescence Turn-on Imaging of Hypochlorous Acid in Living Immune and Cancer Cells," *Chemistry—A European Journal* 22 (2016): 9642–9648, https://doi.org/10.1002/chem.201601270.

33. F. Tian, Y. Jia, Y. Zhang, et al., "A HClO-Specific Near-Infrared Fluorescent Probe for Determination of Myeloperoxidase Activity and Imaging Mitochondrial HClO in Living Cells," *Biosensors and Bioelectronics* 86 (2016): 68–74, https://doi.org/10.1016/j.bios.2016.06.039.

34. Z. Ye, M. Ji, K. Wu, et al., "In-Sequence High-Specificity Dual-Reporter Unlocking of Fluorescent Probe Enables the Precise Identification of Atherosclerotic Plaques," *Angewandte Chemie International Edition* 61 (2022): e202204518, https://doi.org/10.1002/anie.202204518.

35. H. Zheng, W. Peng, M. Liu, S. Zhang, X. Song, and L. Yang, "Ratiometric Fluorescent Probe for Super-Resolution Imaging of Lysosome HClO in Ferroptosis Cells," *Analytical Chemistry* 96 (2024): 11581–11587, https://doi.org/10.1021/acs.analchem.4c02435.

36. L. Shangguan, J. Wang, X. Qian, Y. Wu, and Y. Liu, "Mitochondria-Targeted Ratiometric Chemdosimeter to Detect Hypochlorite Acid for

15213773, 2026, 45, Downloaded from https://onlinelibrary.wiley.com/doi/10.1002/anie.9709775 by Chung-Ang University, Wiley Online Library on [03/11/2026]. See the Terms and Conditions (https://onlinelibrary.wiley.com/terms-and-conditions) on Wiley Online Library for rules of use; OA articles are governed by the applicable Creative Commons License

Monitoring the Drug-Damaged Liver and Kidney," *Analytical Chemistry* 94 (2022): 11881–11888, https://doi.org/10.1021/acs.analchem.2c02431.

37. X. Chen, D. Jiang, C. Jiang, and C. Yao, "A Novel Near-Infrared Ratiometric Fluorescent Probe Targeting Lysosomes for Imaging HOCl In Vitro and In Vivo," *Spectrochimica Acta Part A: Molecular and Biomolecular Spectroscopy* 286 (2023): 121966, https://doi.org/10.1016/j.saa.2022.121966.

38. J. Zielonka, A. Sikora, M. Hardy, J. Joseph, B. P. Dranka, and B. Kalyanaraman, "Boronate Probes as Diagnostic Tools for Real Time Monitoring of Peroxynitrite and Hydroperoxides," *Chemical Research in Toxicology* 25 (2012): 1793–1799, https://doi.org/10.1021/tx300164j.

39. Q. Xu, K.-A. Lee, S. Lee, K. M. Lee, W.-J. Lee, and J. Yoon, "A Highly Specific Fluorescent Probe for Hypochlorous Acid and Its Application in Imaging Microbe-Induced HOCl Production," *Journal of the American Chemical Society* 135 (2013): 9944–9949, https://doi.org/10.1021/ja404649m.

40. Z.-N. Sun, F.-Q. Liu, Y. Chen, P. K. H. Tam, and D. Yang, "A Highly Specific BODIPY-Based Fluorescent Probe for the Detection of Hypochlorous Acid," *Organic Letters* 10 (2008): 2171–2174, https://doi.org/10.1021/ol800507m.

41. K.-I. Setsukinai, Y. Urano, K. Kakinuma, H. J. Majima, and T. Nagano, "Development of Novel Fluorescence Probes That Can Reliably Detect Reactive Oxygen Species and Distinguish Specific Species," *Journal of Biological Chemistry* 278 (2003): 3170–3175, https://doi.org/10.1074/jbc.M209264200.

42. J. Flemmig, J. Remmler, J. Zschaler, and J. Arnhold, "Detection of the Halogenating Activity of Heme Peroxidases in Leukocytes by Aminophenyl Fluorescein," *Free Radical Research* 49 (2015): 768–776, https://doi.org/10.3109/10715762.2014.999676.

43. M. Ren, K. Zhou, L. He, and W. Lin, "Mitochondria and Lysosome-Targetable Fluorescent Probes for HOCl: Recent Advances and Perspectives," *Journal of Materials Chemistry B* 6 (2018): 1716–1733, https://doi.org/10.1039/C7TB03337K.

44. Y. Yue, F. Huo, C. Yin, J. O. Escobedo, and R. M. Strongin, "Recent Progress in Chromogenic and Fluorogenic Chemosensors for Hypochlorous Acid," *Analyst* 141 (2016): 1859–1873, https://doi.org/10.1039/C6AN00158K.

45. T. Yudhistira, S. V. Mulay, Y. Kim, M. B. Halle, and D. G. Churchill, "Imaging of Hypochlorous Acid by Fluorescence and Applications in Biological Systems," *Chemistry—An Asian Journal* 14 (2019): 3048–3084, https://doi.org/10.1002/asia.201900672.

46. S. M. Kondengadan and B. Wang, "Quantitative Factors Introduced in the Feasibility Analysis of Reactive Oxygen Species (ROS)-Sensitive Triggers," *Angewandte Chemie International Edition* 63 (2024): e202403880, https://doi.org/10.1002/anie.202403880.

47. M. Kang, J. Kil, M. M. Fortibui, and M. H. Lee, "Illuminating Hypochlorite: Advances in Fluorescent Probe Design and In Vivo Imaging," *Coordination Chemistry Reviews* 552 (2026): 217505, https://doi.org/10.1016/j.ccr.2025.217505.

48. G. J. Maghzal, K. M. Cergol, S. R. Shengule, et al., "Assessment of Myeloperoxidase Activity by the Conversion of Hydroethidine to 2-Chloroethidium," *Journal of Biological Chemistry* 289 (2014): 5580–5595, https://doi.org/10.1074/jbc.M113.539486.

49. J. K. Hurst, J. M. Albrich, T. R. Green, H. Rosen, and S. Klebanoff, "Myeloperoxidase-Dependent Fluorescein Chlorination by Stimulated Neutrophils," *Journal of Biological Chemistry* 259 (1984): 4812–4821, https://doi.org/10.1016/S0021-9258(17)42918-8.

50. Q. A. Best, N. Sattenapally, D. J. Dyer, C. N. Scott, and M. E. McCarroll, "pH-Dependent Si-Fluorescein Hypochlorous Acid Fluorescent Probe: Spirocycle Ring-Opening and Excess Hypochlorous Acid-Induced Chlorination," *Journal of the American Chemical Society* 135 (2013): 13365–13370, https://doi.org/10.1021/ja401426s.

51. Y. Wang, L. Wu, C. Liu, et al., "A Highly Specific and Ultrasensitive Fluorescent Probe for Basal Lysosomal HOCl Detection Based on Chlorination Induced by Chlorinium Ions (Cl^+)," *Journal of Materials Chemistry B* 5 (2017): 3377–3382, https://doi.org/10.1039/C6TB03345H.

52. E. Bassan, A. Gualandi, P. G. Cozzi, and P. Ceroni, "Design of BODIPY Dyes as Triplet Photosensitizers: Electronic Properties Tailored for Solar Energy Conversion, Photoredox Catalysis and Photodynamic Therapy," *Chemical Science* 12 (2021): 6607–6628, https://doi.org/10.1039/D1SC00732G.

53. S. Jeon, T.-I. Kim, H. Jin, et al., "Amine-Reactive Activated Esters of *Meso*-CarboxyBODIPY: Fluorogenic Assays and Labeling of Amines, Amino Acids, and Proteins," *Journal of the American Chemical Society* 142 (2020): 9231–9239, https://doi.org/10.1021/jacs.9b13982.

54. Y. Cai, C. Gui, K. Samedov, et al., "An Acidic pH Independent Piperazine–TPE AIEgen as a Unique Bioprobe for Lysosome Tracing," *Chemical Science* 8 (2017): 7593–7603, https://doi.org/10.1039/C7SC03515B.

55. A. R. Lippert, G. C. Van de Bittner, and C. J. Chang, "Boronate Oxidation as a Bioorthogonal Reaction Approach for Studying the Chemistry of Hydrogen Peroxide in Living Systems," *Accounts of Chemical Research* 44 (2011): 793–804, https://doi.org/10.1021/ar200126t.

56. A. J. Kettle, C. A. Gedye, M. B. Hampton, and C. C. Winterbourn, "Inhibition of Myeloperoxidase by Benzoic Acid Hydrazides," *Biochemical Journal* 308 (1995): 559–563, https://doi.org/10.1042/bj3080559.

57. K. Pierzchała, M. Pięta, M. Rola, et al., "Fluorescent Probes for Monitoring Myeloperoxidase-Derived Hypochlorous Acid: A Comparative Study," *Scientific Reports* 12 (2022): 9314, https://doi.org/10.1038/s41598-022-13317-8.

58. T. H. de Araujo, S. S. Okada, E. E. B. Ghosn, et al., "Intracellular Localization of Myeloperoxidase in Murine Peritoneal B-Lymphocytes and Macrophages," *Cellular Immunology* 281 (2013): 27–30, https://doi.org/10.1016/j.cellimm.2013.01.002.

59. J. Zhou, L. Li, W. Shi, X. Gao, X. Li, and H. Ma, "HOCl Can Appear in the Mitochondria of Macrophages During Bacterial Infection as Revealed by a Sensitive Mitochondrial-Targeting Fluorescent Probe," *Chemical Science* 6 (2015): 4884–4888, https://doi.org/10.1039/C5SC01562F.

60. X. Xu, Y. Pang, and X. Fan, "Mitochondria in Oxidative Stress, Inflammation and Aging: From Mechanisms to Therapeutic Advances," *Signal Transduction and Targeted Therapy* 10 (2025): 190, https://doi.org/10.1038/s41392-025-02253-4.

61. S. Kongkiatkamon, L. Terkawi, Y. Guan, et al., "Rare Germline Alterations of Myeloperoxidase Predispose to Myeloid Neoplasms," *Leukemia* 36 (2022): 2086–2096, https://doi.org/10.1038/s41375-022-01630-0.

62. L. Liu, P. Wei, W. Yuan, et al., "Detecting Basal Myeloperoxidase Activity in Living Systems With a Near-Infrared Emissive "Turn-On" Probe," *Analytical Chemistry* 92 (2020): 10971–10978, https://doi.org/10.1021/acs.analchem.9b04601.

63. Y. Wang, X. Cheng, N. Yin, et al., "A Hypochlorite-Activated Theranostic Prodrug for Selective Imaging of High Myeloperoxidase Expression Acute Myeloid Leukemia Cells and Drug Release," *Analytical Chemistry* 96 (2024): 12238–12245, https://doi.org/10.1021/acs.analchem.4c00273.

64. N. Aykin-Burns, I. M. Ahmad, Y. Zhu, L. W. Oberley, and D. R. Spitz, "Increased Levels of Superoxide and H_2O_2 Mediate the Differential Susceptibility of Cancer Cells Versus Normal Cells to Glucose Deprivation," *Biochemical Journal* 418 (2009): 29–37, https://doi.org/10.1042/BJ20081258.

65. G.-Y. Liou and P. Storz, "Reactive Oxygen Species in Cancer," *Free Radical Research* 44 (2010): 479–496, https://doi.org/10.3109/10715761003667554.

66. A. Stepanova, C. Konrad, G. Manfredi, R. Springett, V. Ten, and A. Galkin, "The Dependence of Brain Mitochondria Reactive Oxygen Species Production on Oxygen Level Is Linear, Except When Inhibited by Antimycin A," *Journal of Neurochemistry* 148 (2019): 731–745, https://doi.org/10.1111/jnc.14654.

15213773, 2026, 45, Downloaded from https://onlinelibrary.wiley.com/doi/10.1002/anie.9709775 by Chung-Ang University, Wiley Online Library on [03/11/2026]. See the Terms and Conditions (https://onlinelibrary.wiley.com/terms-and-conditions) on Wiley Online Library for rules of use; OA articles are governed by the applicable Creative Commons License

67. H. P. A. Jersmann, D. A. Rathjen, and A. Ferrante, "Enhancement of Lipopolysaccharide-Induced Neutrophil Oxygen Radical Production by Tumor Necrosis Factor Alpha," *Infection and Immunity* 66 (1998): 1744–1747, https://doi.org/10.1128/IAI.66.4.1744-1747.1998.

68. X. Li, L. Yao, Y.-C. Cho, et al., "Alleviation of LPS-Induced Oxidative Stress and Inflammation by Lesbicoumestan (7) via the Increase of Nrf2 Expression in Mouse Kupffer Cells," *Toxicology and Applied Pharmacology* 501 (2025): 117405, https://doi.org/10.1016/j.taap.2025.117405.

69. I. Mellman, R. Fuchs, and A. Helenius, "Acidification of the Endocytic and Exocytic Pathways," *Annual Review of Biochemistry* 55 (1986): 663–700, https://doi.org/10.1146/annurev.bi.55.070186.003311.

70. S. Bazban-Shotorbani, M. M. Hasani-Sadrabadi, A. Karkhaneh, et al., "Revisiting Structure-Property Relationship of pH-Responsive Polymers for Drug Delivery Applications," *Journal of Controlled Release* 253 (2017): 46–63, https://doi.org/10.1016/j.jconrel.2017.02.021.

71. D. G. Russell, B. C. VanderVen, S. Glennie, H. Mwandumba, and R. S. Heyderman, "The Macrophage Marches on Its Phagosome: Dynamic Assays of Phagosome Function," *Nature Reviews Immunology* 9 (2009): 594–600, https://doi.org/10.1038/nri2591.

72. F. Karimi, K. E. S. Locock, J. Chiefari, C. C. Williams, and L. D. Blackman, "Challenges and Opportunities for Cleavable Linkers Used in Polymer−Drug Conjugates," *Journal of the American Chemical Society* 148 (2026): 20297–20321, https://doi.org/10.1021/jacs.6c03661.

73. R. Riedl, A. Kühn, D. Rietz, et al., "Establishment and Characterization of Mild Atopic Dermatitis in the DNCB-Induced Mouse Model," *International Journal of Molecular Sciences* 24 (2023): 12325, https://doi.org/10.3390/ijms241512325.

74. L. Yu and L. Li, "Potential Biomarkers of Atopic Dermatitis," *Frontiers in Medicine* 9 (2022): 1028694, https://doi.org/10.3389/fmed.2022.1028694.

Supporting Information

Additional supporting information can be found online in the Supporting Information section.

The authors have cited additional references within the Supporting Information [75–83].

Supporting File 1: anie74795-sup-0001-SuppMat.pdf.

15213773, 2026, 45, Downloaded from https://onlinelibrary.wiley.com/doi/10.1002/anie.9709775 by Chung-Ang University, Wiley Online Library on [03/11/2026]. See the Terms and Conditions (https://onlinelibrary.wiley.com/terms-and-conditions) on Wiley Online Library for rules of use; OA articles are governed by the applicable Creative Commons License